ACS APPLIED MATERIALS & INTERFACES

Research Article

Cite This: ACS Appl. Mater. Interfaces 2018, 10, 42865−42874

www.acsami.org

Green Synthesis of Porous Cocoon-like rGO for Enhanced Microwave-Absorbing Performances

Shanshan Wang,[†] Yun Zhao,*[,†] Meimei Gao,[†] Haoliang Xue,[†] Yingchun Xu,[†] Caihong Feng,[†] Daxin Shi,[†] Kaihui Liu,[§] and Qingze Jiao*[,†,‡]

[†]School of Chemistry and Chemical Engineering, Beijing Institute of Technology, Beijing 100081, P. R. China

[‡]School of Materials and the Environment, Beijing Institute of Technology, Zhuhai 519085, P. R. China

[§]State Key Laboratory for Mesoscopic Physics, School of Physics, Peking University, Beijing 100871, China

Supporting Information

ABSTRACT: A novel porous cocoon-like reduced graphene oxide (rGO) with high porosity and low density was fabricated by a simple and green reduction reaction using ascorbic acid as the reductant in combination with a freeze-drying process without annealing. The bulk density of porous cocoon-like rGO is only 28.49 mg/cm^3, and the porosity reaches 94.57%. The reaction times have an important influence on the formation of porous cocoon-like rGO and the reduction degree of rGO. The porous cocoon-like rGO exhibits an excellent microwave-absorbing property with a low mass filling ratio of 7.0 wt %; its minimum reflection loss (RL) is −29.05 dB at 15.96 GHz with a sample thickness of 2.0 mm and the effective absorption bandwidth (RL < −10 dB) is 5.27 GHz. The microwave-absorbing property of porous cocoon-like rGO is much better than that of GO and other porous rGO. The in-depth analyses of the reduction degree, porosity, and microwave-absorbing performance illustrate that the microwave-absorbing performance of rGO is significantly related to the reduction degree and porosity. In addition, the synthetic route for porous cocoon-like rGO is simple, has low energy consumption, and is environmentally friendly. Our work demonstrates that the porous cocoon-like rGO is a promising lightweight microwave absorber with high performance.

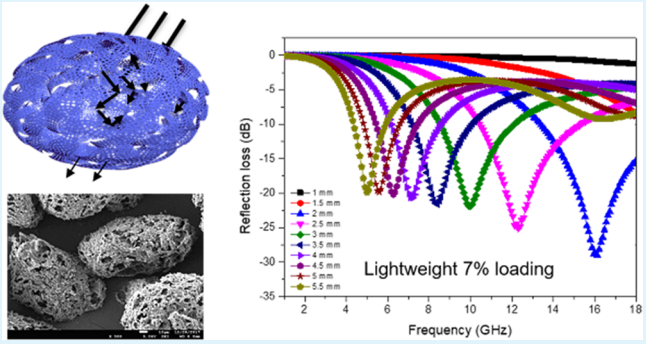

KEYWORDS: *reduced graphene oxide, cocoon-like, porosity, reduction degree, microwave-absorbing performance*

1. INTRODUCTION

Recently, microwave absorbers have been paid more attention because of their important role in information safety and military stealth caused by the electromagnetic radiation pollution.[1−3] These materials are mainly classified as magnetic loss materials (ferrites,[4−6] magnetic metal powders,[7,8] etc.) and dielectric loss materials (SiC,[9,10] ZnO,[11,12] CuS,[13,14] TiO_2,[15−17] etc.). Unfortunately, the high density, large mass filling ratio, narrow bandwidth, and poor environmental adaptability of these materials restrict their practical applications to some extent. Consequently, studies have been focused on the efficient absorbers with thin thickness, light weight, broad bandwidth, powerful absorption, good thermal stability, and antioxidation capability.[18−20]

Carbon materials have attracted more and more attention for their extensive applications.[21−24] As explored in recent years, carbon materials are considered as potential absorber materials because of their lower density, low filling content, high dielectric loss, and environmental stability, including carbon fibers,[25,26] carbon hollow microspheres,[27,28] carbon nanotubes,[29,30] and reduced graphene oxide (rGO).[31] Among these, porous rGO shows an outstanding absorbing performance.[32,33] Kuang et al. prepared rGO with porous network microstructures; the largest absorption intensity was −37.2 dB at 3.5 mm thickness with a loading of 30.0 wt %, and the effective absorption bandwidth (EAB, reflection loss [RL] < −10 dB) was about 3 GHz with a thickness of 2.5 mm.[34] Chen et al. reported that ultralight carbon nanotube/rGO foams exhibited excellent microwave absorption in the range of 2−18 GHz. The minimum RL was −39.5 dB, and the EAB reached up to 16 GHz.[35] Zhang et al. reported that rGO foam obtained using a solvothermal route showed a minimum RL of −34 dB and an EAB of 14.3 GHz.[36] It can be noted that the porous rGO enhances the microwave-absorbing performance because of its low density and unique porous structure, inducing the multireflection loss of microwave.[37] However, such porous rGO exhibits an excellent microwave-absorbing performance with a much higher mass filling ratio of 10.0−30.0 wt %. In addition, the rGO foam is used as a monolithic material, and it shows poor mechanical properties, which limits its application.

Received: September 5, 2018
Accepted: November 19, 2018
Published: November 19, 2018

DOI: 10.1021/acsami.8b15416
ACS Appl. Mater. Interfaces 2018, 10, 42865−42874

Furthermore, the preparation route involves the complicated hydrothermal−solvothermal and annealing process. Moreover, few investigations on the relation between the reduction degree, porosity, and the microwave-absorbing performance have been reported.

Herein, a novel porous cocoon-like rGO was fabricated using a simple and low energy consumption and green reduction reaction with ascorbic acid as the reductant in combination with a freeze-drying process without annealing. The microwave-absorbing performance of porous rGO with different reduction degree and porosity was investigated. The microwave-absorbing performance of porous rGO has been improved with the increase of reduction degree and porosity. The excellent absorption performance, low density, low mass filling ratio, low energy consumption, and the simple and green method are beneficial to practical applications.

2. EXPERIMENTAL

2.1. Materials. Flake graphite of 325 mesh size was provided by Beijing Creative Biological Engineering Materials Co. Ltd. Ascorbic acid was purchased from Beijing Chemicals. All chemicals were of analytical grade and used without any purification.

2.2. Preparation of Ultralight Porous Cocoon-like rGO. GO was obtained using flake graphite as the starting material on the basis of the modified Hummers method.[38] The porous cocoon-like rGO was prepared in a four-neck flask with a mechanical agitator. Briefly, 30 mL of GO (1 mg/mL) aqueous dispersion was sonicated for 30 min. Ascorbic acid (0.12 g) was then added and sonicated for another 10 min. Subsequently, the mixture was transferred into the four-neck flask with continuous stirring at 90 °C and different times (from 0.5 to 2 h); the precipitant was then collected and washed with deionized water. The porous rGO was obtained by a freeze-drying process. The porous cocoon-like rGO was formed after the reaction for 2 h. Therefore, rGO prepared with 0.5, 1, 1.5, and 2 h are labeled as porous rGO 0.5 h, porous rGO 1 h, porous rGO 1.5 h, and porous cocoon-like rGO, respectively.

2.3. Characterization. The morphology was characterized using field emission scanning electron microscopy (FESEM; Hitachi S-4800) and high-resolution transmission electron microscopy (HRTEM; JEM-2010). The crystal structure was examined by X-ray diffraction (XRD; Ultima IV, 40 kV, 150 mA, Cu Kα), Fourier-transform infrared spectroscopy (FTIR; Bruker VECTOR 22, 4000−5000 cm^{-1}), X-ray photoelectron spectroscopy (XPS; PHI 5300X), and Raman spectroscopy (Renishaw, 632.8 nm). The pore structure and porosity of the products were characterized using mercury intrusion porosimetry (AutoPore IV 9510). The bulk density was tested using a measuring cylinder, and the density was calculated as the ratio of mass to volume. The electromagnetic parameters were measured using a vector network analyzer (HP 8722ES) in the range of 1−18 GHz. The GO or rGO was mixed with paraffin at different mass filling ratios and was compressed into coaxial rings with an outer diameter of 7.0 mm, an inner diameter of 3.0 mm, and a thickness of 2.0 mm.

3. RESULTS AND DISCUSSION

The morphologies of the GO, porous rGO with different reaction times, and porous cocoon-like rGO are shown in Figure 1. The reaction time has an obvious effect on the morphology of rGO. In Figure 1a, GO shows a typical flaky morphology. For rGO prepared with a reduction reaction time of 0.5 h (Figure 1b), the size of the rGO sheets decreases and pores appear on the rGO sheets. When GO is reduced for 1 h, the small and porous rGO sheets begin to self-assemble. The products show a certain 3D structure (Figure 1c). As the reaction time increases to 1.5 h, more products with 3D porous structures appear and the product size increases after self-assembly (shown in Figure 1d). In the case of rGO obtained with a reaction time of 2 h (Figure 1e,f), unique 3D porous cocoon-like microstructures with partial overlapping or coalescing of flexible rGO sheets are observed. Not only are the rGO sheets porous but also many large pores are formed in the self-assembly process. Figure 1g,h shows the obvious porous structure and typical transparent tulle-like sheets of porous cocoon-like rGO. Selected-area electron diffraction (SAED, inset in Figure 1h) shows diffraction rings, indicating that rGO sheets are amorphous. Figure 2 shows the preparation procedure of porous cocoon-like rGO.

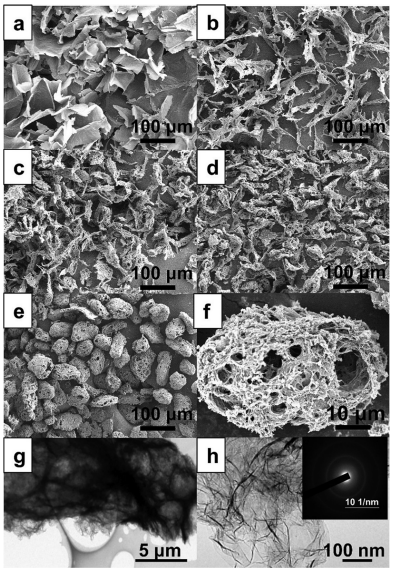

Figure 1. FESEM images of the GO (a), porous rGO 0.5 h (b), porous rGO 1 h (c), porous rGO 1.5 h (d), porous cocoon-like rGO (e,f), and HRTEM images of the porous cocoon-like rGO (g,h). The inset in (h) shows the SAED pattern of porous cocoon-like rGO.

Figure 3 reveals the FTIR spectra of GO and rGO. In Figure 3a, the typical peaks of GO can be observed at 3400 cm^{-1} (O−H stretching vibration), 1722 cm^{-1} (C═O stretching vibrations), 1624 cm^{-1} (C═C stretching of aromatic zooms), 1389 cm^{-1} (−OH stretching vibrations), 1227 cm^{-1} (C−O−C vibrations of epoxy groups), and 1068 cm^{-1} (C−O stretching vibrations).[39] With increasing reduction reaction times, the peak intensities of the above oxygen-containing functional groups for rGO decrease gradually. In the case of rGO 1.5 h and porous cocoon-like rGO (Figure 3d,e), most peaks of oxygen-containing functional groups disappear, which implies that most oxygen-containing functional groups are eliminated during the reduction process. Meanwhile, with the increase of reaction times, the reduction degree of the porous rGO gradually increases. The reduction degree of the product is similar when the reaction time is more than 1.5 h.

The XRD patterns of the samples are given in Figure 4a. Compared to the sharp peak of $2\theta = 11.8°$ for GO, the porous cocoon-like rGO shows a broad weak characteristic peak at $2\theta = 26°$, which is caused by the decrease in the interlayer spacing of rGO. It demonstrates that the oxygen-containing functional groups are effectively eliminated and the rGO sheets have a long-range restacking after reduction by ascorbic acid without annealing.[40] In the typical Raman spectra, two prominent peaks of D and G are observed (Figure 4b). The disorder, defect lattice concentration, and average size of the sp^2 domains of graphitic carbon materials are assessed by the

DOI: 10.1021/acsami.8b15416
ACS Appl. Mater. Interfaces 2018, 10, 42865−42874

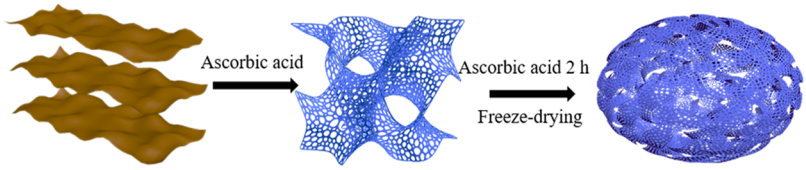

Figure 2. Schematic illustration of the fabrication process for porous cocoon-like rGO.

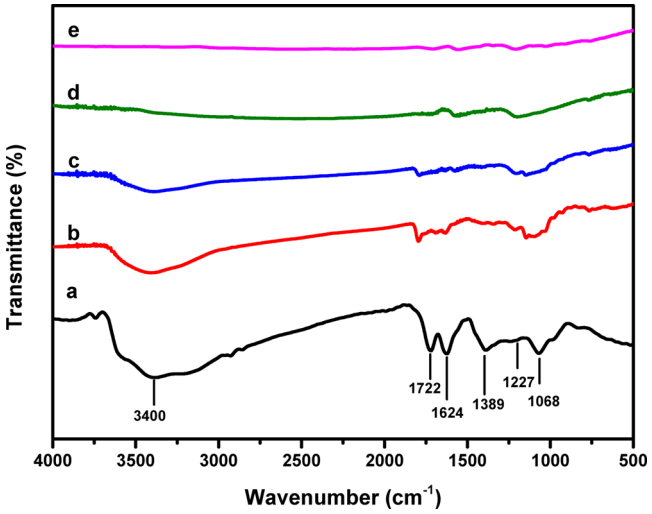

Figure 3. FTIR spectra of the GO (a), porous rGO 0.5 h (b), porous rGO 1 h (c), porous rGO 1.5 h (d), and porous cocoon-like rGO (e).

intensity ratio of D and G peaks (I_D/I_G).[41−44] The I_D/I_G (1.17) of porous cocoon-like rGO is higher than that the GO (0.90), which is regarded as a decrease in the average size of the sp^2 domains upon reduction of the GO, indicating that more lattice defects are introduced and the GO has been successfully changed into rGO after being reduced with ascorbic acid.[45,46]

The compositions of GO and porous cocoon-like rGO are analyzed by XPS. Figure 5a shows only the presence of C1s and O1s peaks at about 284 and 533 eV, respectively. The intensity of O1s is higher than that of C1s, although it is opposite for porous cocoon-like rGO. There are three kinds of C as shown in the C1s peaks of GO in Figure 5b. The binding energies of 284.5, 286.5, and 288.3 eV are assigned to C−C and C═C, C−O, and C═O, respectively.[47] The intensities of C−O and C═O of porous cocoon-like rGO decrease rapidly, suggesting a remarkable reduction after the reduction process (Figure 5c).

Mercury intrusion porosimetry is used to estimate the pore size distribution and porosity of the porous rGO. The pore size distributions of the rGO obtained by reacting for 1, 1.5, and 2 h are shown in Figure 6. The pore size distribution profiles with peaks at 0.5−330 μm are observed for all these porous rGOs, and the pores with diameters of 50−330 μm increase with the increase of reaction times. This may be due to the self-assembly of rGO sheets, which leads to the formation of larger pores. The porosity and bulk density of the porous rGO are shown in Table 1. The porosity of rGO increases and the bulk density of rGO decreases with increasing reaction times. As shown in Figure 6 and Table 1, the porous cocoon-like rGO prepared with a reaction time of 2 h possesses extensive pore size distribution and the highest porosity (94.57%). Furthermore, the bulk density of porous cocoon-like rGO is only 28.49 mg/cm^3, which is conducive to the practical application of absorbing materials.

The electromagnetic parameters are important for the microwave-absorbing material. Because the magnetic properties of GO and porous rGO are ignorable, the magnetic loss can be negligible. As predicted in Figure S1, the permeability real part (μ') for all samples is close to 1 and the values of permeability imaginary part (μ'') fluctuate and are around 0. It can be noted from the magnetic loss tangent curve that the magnetic losses are almost 0. Figure 7 depicts the permittivity of the samples with different reaction times at a loading of 7.0 wt %. In Figure 7, the permittivity real part (ε'), permittivity imaginary part (ε''), and dielectric loss tangent ($\tan \delta = \varepsilon''/\varepsilon'$) for porous rGO are obviously higher than those of GO in 1−18 GHz. When the reaction time is not longer than 1.5 h, the ε', ε'', and tan δ become larger with the increase in reaction

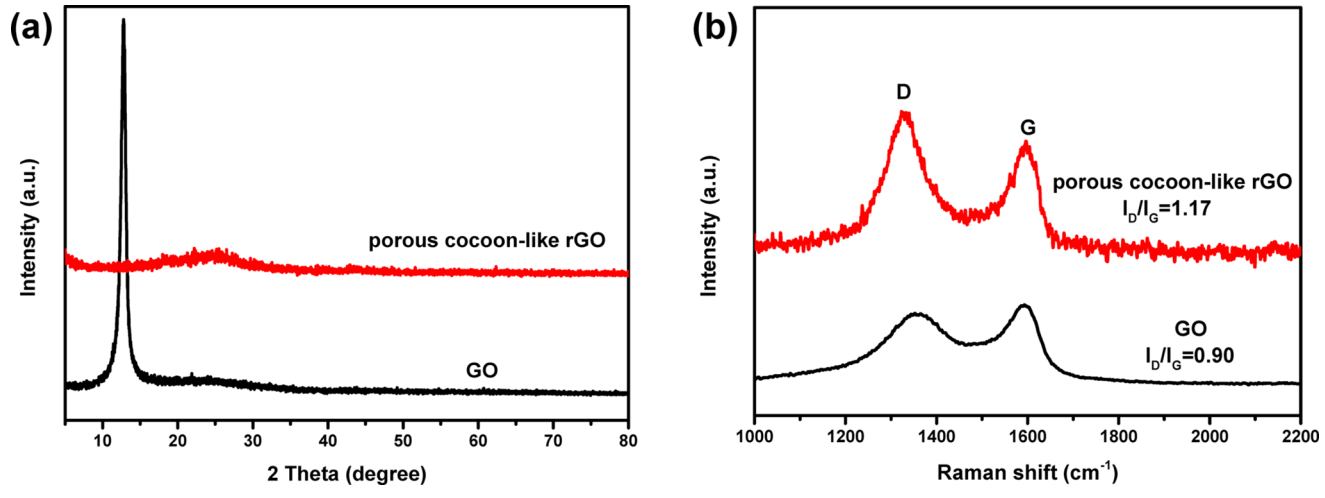

Figure 4. XRD patterns of GO and porous cocoon-like rGO (a) and Raman spectra of GO and porous cocoon-like rGO (b).

DOI: 10.1021/acsami.8b15416
ACS Appl. Mater. Interfaces 2018, 10, 42865−42874

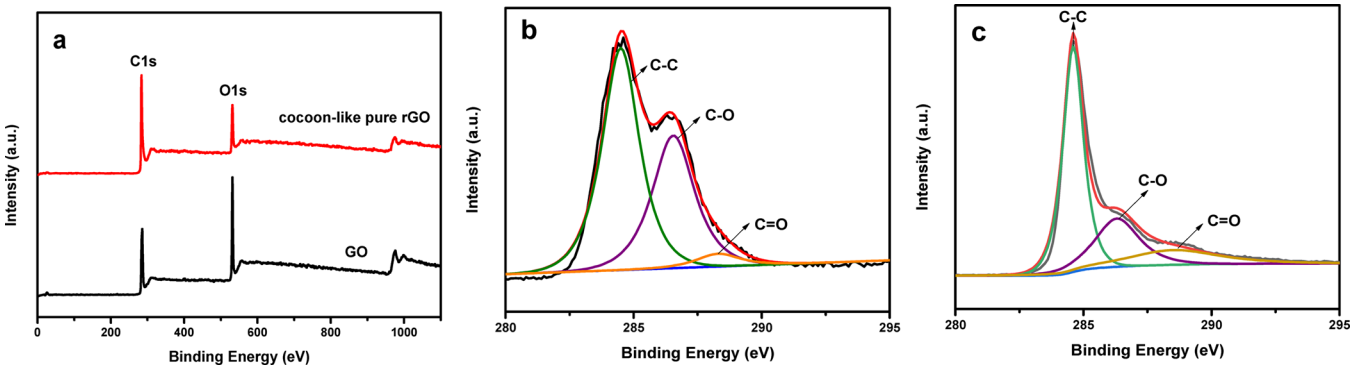

Figure 5. XPS spectra of survey scan of GO and porous cocoon-like rGO (a), C1s of GO (b), and C1s of porous cocoon-like rGO (c).

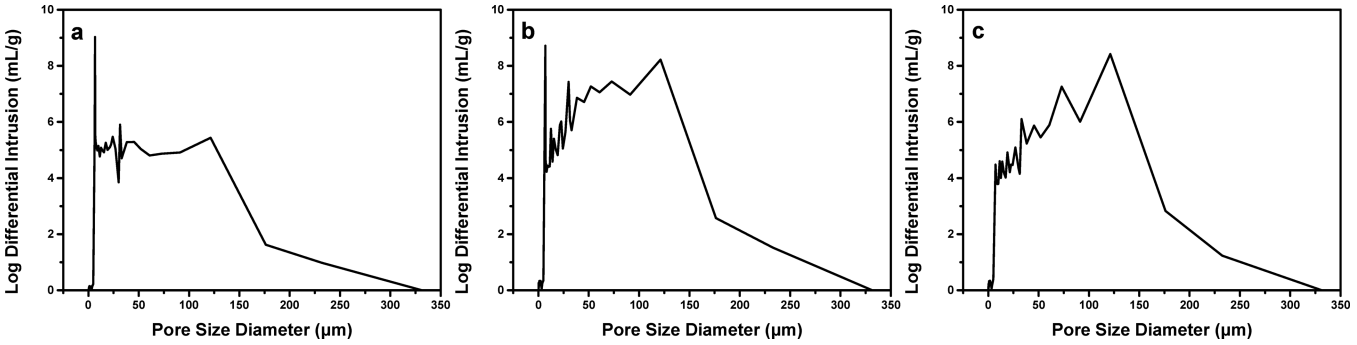

Figure 6. Pore size distribution of porous rGO 1 h (a), porous rGO 1.5 h (b), and porous cocoon-like rGO (c).

Table 1. Porosity and Bulk Density of the Porous rGO

sample	porosity (%)	bulk density (mg/cm^3)
porous rGO 1 h	79.98	61.13
porous rGO 1.5 h	84.31	32.91
porous cocoon-like rGO	94.57	28.49

time. This is due to the chemical reduction process improving the electrical conductivity. On the basis of the free-electron theory, the strong dielectric loss of materials results from the high conductivity.[11] The values of ε', ε'', and tan δ for porous cocoon-like rGO are not the largest, although the reduction reaction time is the longest. Compared with other porous rGOs, the porous cocoon-like rGO has formed a special morphology with increased size, which makes the resistance increase between the particles and leads to the decrease of dielectric constant and dielectric loss.

The RL of the samples can be calculated according to the three equations[48]

$$\mathrm{RL(dB)} = 20 \log \left| \frac{z_{in} - z_0}{z_{in} + z_0} \right| \quad (1)$$

$$z_{in} = z_0 \sqrt{\frac{\mu_r}{\varepsilon_r}} \tan h\left(j \frac{2\pi f d}{c} \sqrt{\mu_r \varepsilon_r} \right) \quad (2)$$

$$\varepsilon_r = \varepsilon' - j\varepsilon'', \quad \mu_r = \mu' - j\mu'' \quad (3)$$

where z_{in} is the normalized input impedance, z_0 is the free space impedance, ε_r and μ_r are the relative complex permittivity and permeability of the absorbers, respectively, f is the frequency of microwave, d is the sample thickness, and c is the microwave velocity in vacuum.

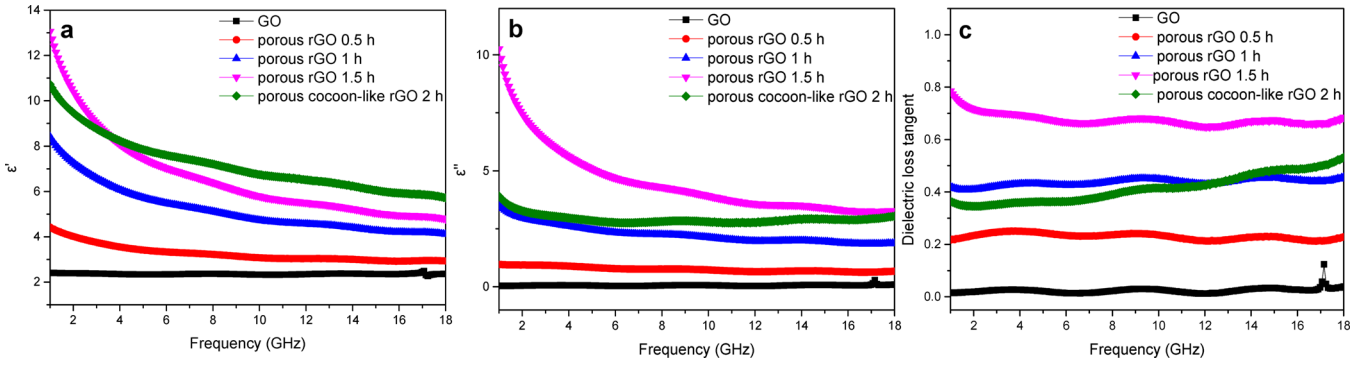

Figure 7. Permittivity real part (a), permittivity imaginary part (b), and dielectric loss tangent (c) of GO, porous rGO, and porous cocoon-like rGO.

DOI: 10.1021/acsami.8b15416
ACS Appl. Mater. Interfaces 2018, 10, 42865−42874

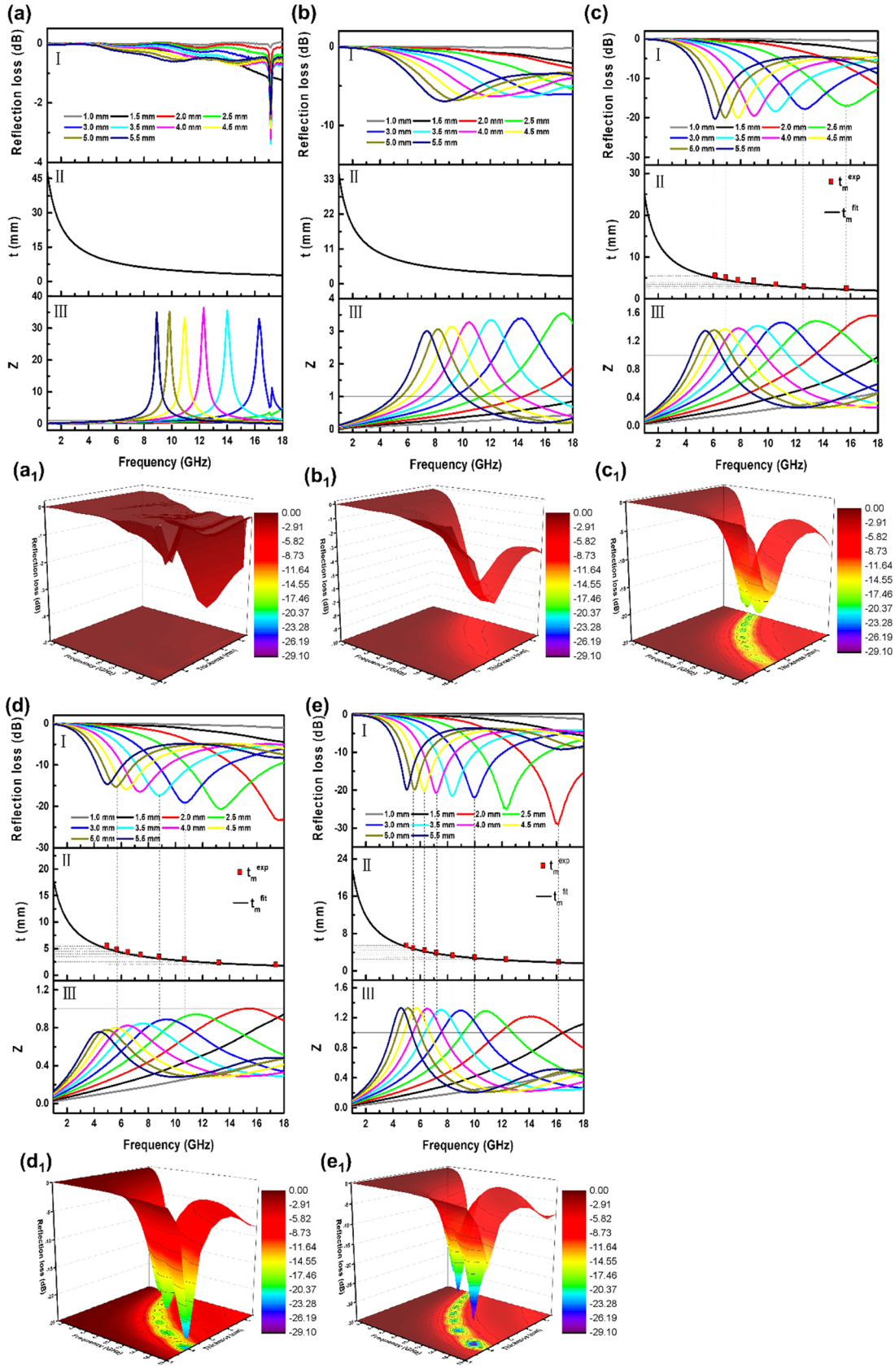

Figure 8. The calculated 2D/3D RL with different thicknesses (a(I)−e(I),a_1−e_1), simulations of the absorber thickness (t_m) versus peak frequency (f_m) under n = 1 (a(II)−e(II)), the relationship between the impedance matching characteristics ($Z = |Z_{in}/Z_0|$) and the frequency (a(III)−e(III)) of GO (a,a_1), porous rGO 0.5 h (b,b_1), porous rGO 1 h (c,c_1), porous rGO 1.5 h (d,d_1), and porous cocoon-like rGO (e,e_1).

DOI: 10.1021/acsami.8b15416
ACS Appl. Mater. Interfaces 2018, 10, 42865−42874

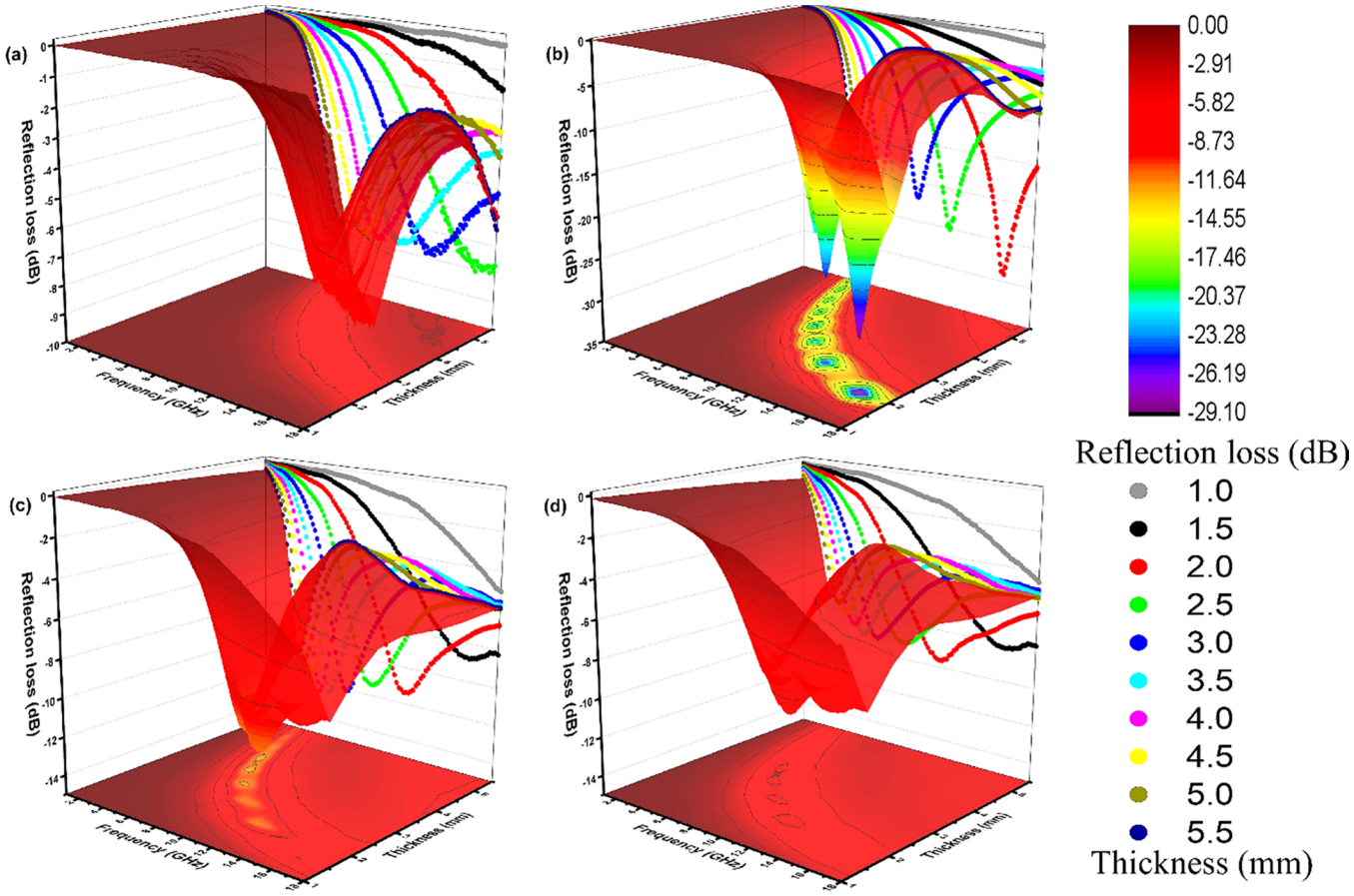

Figure 9. The calculated 2D/3D RL dependence on the frequency and the thickness of the porous cocoon-like rGO with mass filling ratios of 5.5 (a), 7.0 (b), 8.5 (c), and 10.0 wt % (d).

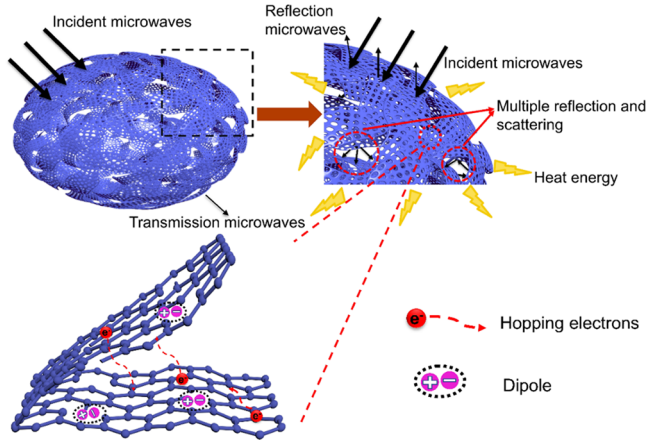

Figure 10. Schematic illustration of the microwave-absorption mechanism of porous cocoon-like rGO.

Figure 8 exhibits the two-dimensional (2D) and three-dimensional (3D) RL curves of these GO and rGO samples with a mass filling ratio of 7.0 wt % at different thicknesses. As shown in Figure 8a-(I),a_1, the GO is almost invalid for microwave with different thicknesses. Compared to GO, the microwave-absorbing performance of the porous rGO 0.5 h is enhanced a little as shown in Figure 8b-(I),b_1, whereas the microwave-absorbing performances of the porous rGO 1 h and rGO 1.5 h are enhanced obviously (Figure 8c-(I),c_1 and 8d-(I),d_1). The minimum RL of the porous rGO 1 h is −20.2 dB at 5.5 mm thickness, and the EAB reaches 5.35 GHz at 3.0 mm. In Figure 8d-(I),d_1, the minimum RL of porous rGO 1.5 h is −23.39 dB with a thickness of 2.0 mm at 17.83 GHz and the EAB reaches 6.71 GHz at 2.5 mm. As shown in Figure 8e-(I),e_1, the porous cocoon-like rGO shows the strongest absorption peak. The minimum RL of the porous cocoon-like rGO reaches −29.05 dB with a thickness of 2.0 mm at 15.96 GHz, and the EAB is 5.27 GHz at a thickness of 2.5 mm.

It's obvious that the microwave-absorbing performance is sensitive to the thickness. When the thickness is increased, the minimum RL moves to lower frequency. The result can be explained using the quarter-wavelength matching model. The peak frequency (f_m) and the absorber thickness (t_m) satisfy the matching equation:[49]

$$t_m = nc/(4f_m\sqrt{|\varepsilon_r||\mu_r|}) \quad (\text{where } n = 1, 3, 5, \ldots) \tag{4}$$

When t_m and f_m satisfy this equation, the incident and reflected waves in the absorbers are out of phase by 180°, leading to an extinction of the waves at the air−absorber interface. In this case, the minimum RL reaches the maximum value.[30] As shown in Figure 8c(II)−e(II), the matching thicknesses (t_m^{exp}) are achieved from the RL curve marked with red square. The t_m (t_m^{fit}) can be simulated according to eq 4. Obviously, all the experimental results are in accordance with the curve, which implies that the microwave-absorbing performances of the porous rGO 1 h, porous rGO 1.5 h, and porous cocoon-like rGO obey the quarter-wavelength matching model.

DOI: 10.1021/acsami.8b15416
ACS Appl. Mater. Interfaces 2018, 10, 42865−42874

Table 2. Microwave-Absorbing Performances of Carbon-Based Materials Reported in Recent Years

absorber	mass filling ratio (wt %)	minimum RL (dB)	thickness (mm)	EAB (GHz)	ref
PCHMs	20.0	−84	3.9	4.8	28
rGO	30.0	−37.2	3.5		34
NG	30.0	−11.3	3.0	2.1	57
graphene microflowers	10.0	−42.9	4.0	5.59	58
MWCNT/CGFs	100.0	−39.5	10.0	16	35
CNPs/rGO	40.0	−43.4	1.5	3.6	59
$NiFe_2O_4$-h/G	15.0	−40.9	3.5	2.8	60
CoNi/NG	30.0	−22	2.0		8
$NiCo_2$/GNS	50.0	−30	1.6		61
Fe_3O_4@LAS/rGO	50.0	−65	2.1	4	62
MoS_2/GN	15.0	−55.3	5.6	1.6	63
rGO/h-BN	25.0	−40.5	1.6	5	18
porous cocoon-like rGO	7.0	−29.05	2.0	5.27	this work

Moreover, the impedance matching is another important factor for the absorbers to enhance the microwave absorption property.[50,51] As shown in eqs 1 and 2, when the materials achieve a good impedance matching ($Z = |Z_{in}/Z_0|$ is equal or close to 1), more microwaves can enter the absorbers and then will be converted to heat or attenuated through interference; therefore, the best absorbing property could be obtained.[28,52] Figure 8a(III)−e(III) shows the Z curves of GO and porous rGO with different thicknesses. In Figure 8a(III), the values of Z of GO are much greater than 1 for different thicknesses. It indicates that the product is impedance mismatched. Therefore, the lowest dielectric loss and serious impedance mismatch of the GO result in very poor microwave absorption performances. In Figure 8b(III)−d(III), all the values of the porous rGO are significantly lower than that of the GO, the maximum values of the porous rGO are getting closer and closer to 1, and the values of Z near 1 correspond to the strongest absorption. It implies that the high performance of absorbers is dependent on the well-matched impedance. It is the result of the impedance match caused by appropriate permittivity, which is attributed to the high degree of reduction of rGO. In Figure 8e-(III), the maximum values of the porous cocoon-like rGO are slightly bigger than those of the porous rGO 1.5 h, but they are also close to 1. The increased maximum values of Z for the porous cocoon-like rGO are due to the decreased permittivity, which is caused by the change in the morphology and size of porous cocoon-like rGO. Porous cocoon-like rGO shows a strong absorption as shown in Figure 8e-(I). Comparing the porous cocoon-like rGO to the porous rGO 1.5 h, their reduction degrees are similar, although the porous cocoon-like rGO exhibits the strongest absorption. It is attributed to the highest porosity resulting from the unique morphology of the porous cocoon-like rGO. Hence, the waves can suffer multiple reflection and scattering loss in the inner space of the porous cocoon-like rGO to improve the absorption performance.[53]

The 2D/3D RL curves of the samples with different mass filling ratios of porous cocoon-like rGO are shown in Figure 9. Clearly, the mass filling ratio has a great effect on the microwave-absorbing performance. As shown in Figure 9a, the sample with 5.5 wt % porous cocoon-like rGO is almost invalid for microwave, and the minimum RL only reaches −8.85 dB at 14.61 GHz. The microwave-absorbing performance of the porous cocoon-like rGO with a mass filling ratio of 7.0 wt % is enhanced obviously (Figure 9b). Its minimum RL reaches −29.05 dB at 15.96 GHz and a thickness of 2.0 mm, and the EAB (RL < −10 dB) is 5.27 GHz. The microwave-absorbing performances of the samples decrease with the further increase of mass filling ratios. In Figure 9c, the minimum RL of the samples with a mass filling ratio of 8.5 wt % reaches −12.45 dB at 5.42 GHz with a thickness of 4.0 mm, and the EAB is 2.5 GHz with a thickness of 2.5 mm. When the mass filling ratio of the porous cocoon-like rGO is increased to 10.0 wt %, the minimum RL of the sample reaches −9.62 dB at 11.54 GHz with a thickness of 2.0 mm (Figure 9d). The results can also be explained using the impedance matching characteristic. As shown in Figure S2b(III), the values of Z of the porous cocoon-like rGO with a mass filling ratio of 7.0 wt % are close to 1 with the well-matched impedance. The inappropriate permittivity caused by the lower and the higher mass filling ratios results in the impedance mismatch, which leads to the bad microwave-absorbing properties. Therefore, the optimum mass filling ratio is 7.0 wt %.

The microwave-absorbing mechanism of porous cocoon-like rGO is shown in Figure 10. First, the impedance match plays an important role in the good microwave-absorbing performance of porous cocoon-like rGO. The high degree of reduction and the special porous and cocoon-like structure of the sample with low density lead to a good impedance match with a much lower mass filling ratio. Therefore, more microwaves enter the interior of the sample and can be absorbed. Second, as mentioned above, there are some defects on the rGO sheets, which act as polarized centers and improve the dielectric loss, thus enhancing the microwave-absorbing performance.[54] Furthermore, comparing with rGO sheets, the porous cocoon-like rGO shows a 3D structure. In other words, it is a conductive network and the hopping electrons occur between the rGO sheets, which results in a higher conductive loss.[9,34,55] Moreover, the porous structure formed by assembled rGO sheets and the pores on rGO sheets cause multiple reflection and scattering of microwaves on the surface of rGO sheets; therefore, most microwaves are converted into heat energy and dissipated.[54,56]

The microwave-absorbing performances of carbon-based materials reported in the recent literature are summarized in Table 2. Porous cocoon-like rGO in this work exhibits an effective absorption, and the absorption bandwidth is better than most materials with a much lower mass filling ratio at a rather thin thickness, suggesting the porous cocoon-like rGO is a promising candidate as a thin and lightweight microwave absorber.

DOI: 10.1021/acsami.8b15416
ACS Appl. Mater. Interfaces 2018, 10, 42865−42874

4. CONCLUSIONS

In summary, we reported a novel porous cocoon-like rGO as a microwave absorber. The rGO displays a special porous cocoon-like morphology, a high porosity of 94.57%, a very low density of 28.49 mg/cm^3, and an excellent microwave-absorbing property with a low mass filling ratio. The minimum RL is −29.05 dB at 2.0 mm thickness with a mass filling ratio of 7.0 wt %, and the EAB is 5.27 GHz with a thickness of 2.5 mm. The microwave-absorbing performance of porous cocoon-like rGO is much better than that of GO and other porous rGOs. The high reduction degree and porosity are important for enhancing the microwave-absorbing performances. The porous cocoon-like rGO prepared using an environmentally friendly route is promising as a practical microwave absorption material.

■ ASSOCIATED CONTENT

Supporting Information

The Supporting Information is available free of charge on the ACS Publications website at DOI: 10.1021/acsami.8b15416.

The permeability real part (μ'), permeability imaginary part (μ''), and magnetic loss tangent of the GO and porous cocoon-like rGO, the RL curves with different thicknesses, simulations of the absorber thickness (t_m) versus peak frequency (f_m) under n = 1, the relationship between the impedance matching characteristics (Z = $|Z_{in}/Z_0|$), and the frequency of porous cocoon-like rGO with different mass filling ratios (PDF)

■ AUTHOR INFORMATION

Corresponding Authors

*E-mail: zhaoyun@bit.edu.cn. Tel: +86-10-68918979 (Y.Z.).
*E-mail: jiaoqz@bit.edu.cn (Q.J.).

ORCID

Yun Zhao: 0000-0002-4432-9305
Caihong Feng: 0000-0002-2825-0904
Kaihui Liu: 0000-0002-8781-2495

Author Contributions

All authors have given approval to the final version of the manuscript.

Notes

The authors declare no competing financial interest.

■ ACKNOWLEDGMENTS

The authors of this paper would like to thank the National Natural Science Foundation of China (no. 21376029) and the Analysis & Testing Center, Beijing Institute of Technology for sponsoring this research.

■ REFERENCES

(1) Estévez, D.; Qin, F.; Quan, L.; Luo, Y.; Zheng, X. F.; Wang, H.; Peng, H. X. Complementary Design of Nano-Carbon/Magnetic Microwire Hybrid Fibers for Tunable Microwave Absorption. *Carbon* **2018**, *132*, 486−494.

(2) Zhao, H.; Cheng, Y.; Ma, J.; Zhang, Y.; Ji, G.; Du, Y. A Sustainable Route from Biomass Cotton to Construct Lightweight and High-Performance Microwave Absorber. *Chem. Eng. J.* **2018**, *339*, 432−441.

(3) Ma, J.; Wang, X.; Cao, W.; Han, C.; Yang, H.; Yuan, J.; Cao, M. A Facile Fabrication and Highly Tunable Microwave Absorption of 3D Flower-Like Co_3O_4-rGO Hybrid-Architectures. *Chem. Eng. J.* **2018**, *339*, 487−498.

(4) Liu, Y.; Fu, Y.; Liu, L.; Li, W.; Guan, J.; Tong, G. Low-Cost Carbothermal Reduction Preparation of Monodisperse Fe_3O_4/C Core−Shell Nanosheets for Improved Microwave Absorption. *ACS Appl. Mater. Interfaces* **2018**, *10*, 16511.

(5) Lv, H.; Liang, X.; Cheng, Y.; Zhang, H.; Tang, D.; Zhang, B.; Ji, G.; Du, Y. Coin-like α-Fe_2O_3@$CoFe_2O_4$ Core−Shell Composites with Excellent Electromagnetic Absorption Performance. *ACS Appl. Mater. Interfaces* **2015**, *7*, 4744−4750.

(6) Liu, Y.; Chen, Z.; Zhang, Y.; Feng, R.; Chen, X.; Xiong, C.; Dong, L. Broadband and Lightweight Microwave Absorber Constructed by in Situ Growth of Hierarchical $CoFe_2O_4$/Reduced Graphene Oxide Porous Nanocomposites. *ACS Appl. Mater. Interfaces* **2018**, *10*, 13860−13868.

(7) Li, H.; Cao, Z.; Lin, J.; Zhao, H.; Jiang, Q.; Jiang, Z.; Liao, H.; Kuang, Q.; Xie, Z. Synthesis of U-Channelled Spherical $Fe_x(Co_yNi_{1-y})_{100-x}$ Janus Colloidal Particles with Excellent Electromagnetic Wave Absorption Performance. *Nanoscale* **2018**, *10*, 1930−1938.

(8) Feng, J.; Pu, F.; Li, Z.; Li, X.; Hu, X.; Bai, J. Interfacial Interactions and Synergistic Effect of CoNi Nanocrystals and Nitrogen-Doped Graphene in a Composite Microwave Absorber. *Carbon* **2016**, *104*, 214−225.

(9) Han, M.; Yin, X.; Hou, Z.; Song, C.; Li, X.; Zhang, L.; Cheng, L. Flexible and Thermostable Graphene/SiC Nanowire Foam Composites with Tunable Electromagnetic Wave Absorption Properties. *ACS Appl. Mater. Interfaces* **2017**, *9*, 11803−11810.

(10) Yan, L.; Hong, C.; Sun, B.; Zhao, G.; Cheng, Y.; Dong, S.; Zhang, D.; Zhang, X. In Situ Growth of Core−Sheath Heterostructural SiC Nanowire Arrays on Carbon Fibers and Enhanced Electromagnetic Wave Absorption Performance. *ACS Appl. Mater. Interfaces* **2017**, *9*, 6320−6331.

(11) Song, C.; Yin, X.; Han, M.; Li, X.; Hou, Z.; Zhang, L.; Cheng, L. Three-Dimensional Reduced Graphene Oxide Foam Modified with ZnO Nanowires for Enhanced Microwave Absorption Properties. *Carbon* **2017**, *116*, 50−58.

(12) Feng, W.; Wang, Y.; Chen, J.; Guo, L.; Ouyang, J.; Jia, D.; Zhou, Y. Microwave Absorbing Property Optimization of Starlike ZnO/Reduced Graphene Oxide Doped by ZnO Nanocrystal Composites. *Phys. Chem. Chem. Phys.* **2017**, *19*, 14596−14605.

(13) Zhao, B.; Shao, G.; Fan, B.; Zhao, W.; Xie, Y.; Zhang, R. Synthesis of Flower-Like CuS Hollow Microspheres Based on Nanoflakes Self-Assembly and Their Microwave Absorption Properties. *J. Mater. Chem. A* **2015**, *3*, 10345−10352.

(14) Wei, Y.-Z.; Wang, G.-S.; Wu, Y.; Yue, Y.-H.; Wu, J.-T.; Lu, C.; Guo, L. Bioinspired Design and Assembly of Platelet Reinforced Polymer Films with Enhanced Absorption Properties. *J. Mater. Chem. A* **2014**, *2*, 5516−5524.

(15) Xu, J.; Qi, X.; Sun, Y.; Wang, Z.; Liu, Y.; Luo, C.; Li, B.; Zhong, W.; Fu, Q.; Pan, C. Tuning the Electromagnetic Synergistic Effects for Enhanced Microwave Absorption via Magnetic Nickel Core Encapsulated in Hydrogenated Anatase TiO_2 Shell. *ACS Sustainable Chem. Eng.* **2018**, *6*, 12046−12054.

(16) Xu, J.; Qi, X.; Luo, C.; Qiao, J.; Xie, R.; Sun, Y.; Zhong, W.; Fu, Q.; Pan, C. Synthesis and Enhanced Microwave Absorption Properties: A Strongly Hydrogenated TiO_2 Nanomaterial. *Nanotechnology* **2017**, *28*, 425701.

(17) Tian, L.; Xu, J.; Just, M.; Green, M.; Liu, L.; Chen, X. Broad Range Energy Absorption Enabled by Hydrogenated TiO_2 Nanosheets: From Optical to Infrared and Microwave. *J. Mater. Chem. C* **2017**, *5*, 4645−4653.

(18) Kang, Y.; Jiang, Z.; Ma, T.; Chu, Z.; Li, G. Hybrids of Reduced Graphene Oxide and Hexagonal Boron Nitride: Lightweight Absorbers with Tunable and Highly Efficient Microwave Attenuation Properties. *ACS Appl. Mater. Interfaces* **2016**, *8*, 32468−32476.

(19) Wang, Y.; Wu, X.; Zhang, W.; Luo, C.; Li, J.; Wang, Q.; Wang, Q. Synthesis of Polyaniline Nanorods and Fe_3O_4 Microspheres on Graphene Nanosheets and Enhanced Microwave Absorption Performances. *Mater. Chem. Phys.* **2018**, *209*, 23−30.

DOI: 10.1021/acsami.8b15416
ACS Appl. Mater. Interfaces 2018, 10, 42865−42874

(20) Zhang, K.; Zhang, Q.; Gao, X.; Chen, X.; Wang, Y.; Li, W.; Wu, J. Effect of Absorbers' Composition on the Microwave Absorbing Performance of Hollow Fe_3O_4 Nanoparticles Decorated CNTs/Graphene/C Composites. *J. Alloys Compd.* **2018**, *748*, 706−716.
(21) Zhang, L.; Liu, W.; Shi, W.; Xu, X.; Mao, J.; Li, P.; Ye, C.; Yin, R.; Ye, S.; Liu, X.; Cao, X.; Gao, C. Boosting Lithium Storage Properties of MOF Derivatives through a Wet-Spinning Assembled Fiber Strategy. *Chem. - Eur. J.* **2018**, *24*, 13792−13799.
(22) Guan, B. Y.; Yu, X. Y.; Wu, H. B.; Lou, X. W. Complex Nanostructures from Materials Based on Metal-Organic Frameworks for Electrochemical Energy Storage and Conversion. *Adv. Mater.* **2017**, *29*, 1703614.
(23) Xu, X.; Shi, W.; Li, P.; Ye, S.; Ye, C.; Ye, H.; Lu, T.; Zheng, A.; Zhu, J.; Xu, L.; Zhong, M.; Cao, X. Facile Fabrication of Three-Dimensional Graphene and Metal−Organic Framework Composites and Their Derivatives for Flexible All-Solid-State Supercapacitors. *Chem. Mater.* **2017**, *29*, 6058−6065.
(24) Lu, Y.; Gong, Q.; Lu, F.; Liang, J.; Ji, L.; Nie, Q.; Zhang, X. Preparation of Sulfonated Porous Carbon Nanotubes/Activated Carbon Composite Beads and Their Adsorption of Low Density Lipoprotein. *J. Mater. Sci.: Mater. Med.* **2011**, *22*, 1855−1862.
(25) Zhan, Y.; Long, Z.; Wan, X.; Zhang, J.; He, S.; He, Y. 3D Carbon Fiber Mats/Nano-Fe_3O_4 Hybrid Material with High Electromagnetic Shielding Performance. *Appl. Surf. Sci.* **2018**, *444*, 710−720.
(26) Shah, A.; Ding, A.; Wang, Y.; Zhang, L.; Wang, D.; Muhammad, J.; Huang, H.; Duan, Y.; Dong, X.; Zhang, Z. Enhanced Microwave Absorption by Arrayed Carbon Fibers and Gradient Dispersion of Fe Nanoparticles in Epoxy Resin Composites. *Carbon* **2016**, *96*, 987−997.
(27) Xu, H.; Yin, X.; Li, M.; Ye, F.; Han, M.; Hou, Z.; Li, X.; Zhang, L.; Cheng, L. Mesoporous Carbon Hollow Microspheres with Red Blood Cell Like Morphology for Efficient Microwave Absorption at Elevated Temperature. *Carbon* **2018**, *132*, 343−351.
(28) Xu, H.; Yin, X.; Zhu, M.; Han, M.; Hou, Z.; Li, X.; Zhang, L.; Cheng, L. Carbon Hollow Microspheres with a Designable Mesoporous Shell for High-Performance Electromagnetic Wave Absorption. *ACS Appl. Mater. Interfaces* **2017**, *9*, 6332−6341.
(29) Zhang, S.; Qi, Z.; Zhao, Y.; Jiao, Q.; Ni, X.; Wang, Y.; Chang, Y.; Ding, C. Core/Shell Structured Composites of Hollow Spherical $CoFe_2O_4$ and CNTs as Absorbing Materials. *J. Alloys Compd.* **2017**, *694*, 309−312.
(30) Yin, Y.; Liu, X.; Wei, X.; Yu, R.; Shui, J. Porous CNTs/Co Composite Derived from Zeolitic Imidazolate Framework: A Lightweight, Ultrathin, and Highly Efficient Electromagnetic Wave Absorber. *ACS Appl. Mater. Interfaces* **2016**, *8*, 34686−34698.
(31) Zhang, Y.; Huang, Y.; Zhang, T.; Chang, H.; Xiao, P.; Chen, H.; Huang, Z.; Chen, Y. Broadband and Tunable High-Performance Microwave Absorption of an Ultralight and Highly Compressible Graphene Foam. *Adv. Mater.* **2015**, *27*, 2049−2053.
(32) Geim, A. K.; Novoselov, K. S. The Rise of Graphene. *Nat. Mater.* **2007**, *6*, 183−191.
(33) Kou, L.; Liu, Y.; Zhang, C.; Shao, L.; Tian, Z.; Deng, Z.; Gao, C. A Mini Review on Nanocarbon-Based 1D Macroscopic Fibers: Assembly Strategies and Mechanical Properties. *Nano-Micro Lett.* **2017**, *9*, 51.
(34) Kuang, B.; Song, W.; Ning, M.; Li, J.; Zhao, Z.; Guo, D.; Cao, M.; Jin, H. Chemical Reduction Dependent Dielectric Properties and Dielectric Loss Mechanism of Reduced Graphene Oxide. *Carbon* **2018**, *127*, 209−217.
(35) Chen, H.; Huang, Z.; Huang, Y.; Zhang, Y.; Ge, Z.; Qin, B.; Liu, Z.; Shi, Q.; Xiao, P.; Yang, Y.; Zhang, T.; Chen, Y. Synergistically Assembled MWCNT/Graphene Foam with Highly Efficient Microwave Absorption in Both C and X Bands. *Carbon* **2017**, *124*, 506−514.
(36) Zhang, Y.; Huang, Y.; Chen, H.; Huang, Z.; Yang, Y.; Xiao, P.; Zhou, Y.; Chen, Y. Composition and Structure Control of Ultralight Graphene Foam for High-Performance Microwave Absorption. *Carbon* **2016**, *105*, 438−447.
(37) Chen, X.; Chen, J.; Meng, F.; Shan, L.; Jiang, M.; Xu, X.; Lu, J.; Wang, Y.; Zhou, Z. Hierarchical Composites of Polypyrrole/Graphene Oxide Synthesized by in Situ Intercalation Polymerization for High Efficiency and Broadband Responses of Electromagnetic Absorption. *Compos. Sci. Technol.* **2016**, *127*, 71−78.
(38) Hummers, W. S., Jr.; Offeman, R. E. Preparation of Graphitic Oxide. *J. Am. Chem. Soc.* **1958**, *80*, 1339.
(39) Wu, Y.; Yi, N.; Huang, L.; Zhang, T.; Fang, S.; Chang, H.; Li, N.; Oh, J.; Lee, J. A.; Kozlov, M.; et al. Three-Dimensionally Bonded Spongy Graphene Material with Super Compressive Elasticity and Near-Zero Poisson's Ratio. *Nat. Commun.* **2015**, *6*, 6141.
(40) Zhao, B.; Shao, G.; Fan, B.; Zhao, W.; Zhang, R. Investigation of the Electromagnetic Absorption Properties of Ni@TiO_2 and Ni@SiO_2 Composite Microspheres with Core−Shell Structure. *Phys. Chem. Chem. Phys.* **2015**, *17*, 2531−2539.
(41) Zhang, L.; Zhang, F.; Yang, X.; Long, G.; Wu, Y.; Zhang, T.; Leng, K.; Huang, Y.; Ma, Y.; Yu, A.; et al. Porous 3D Graphene-Based Bulk Materials with Exceptional High Surface Area and Excellent Conductivity for Supercapacitors. *Sci. Rep.* **2013**, *3*, 1408.
(42) Ferrari, A. C.; Robertson, J. Interpretation of Raman Spectra of Disordered and Amorphous Carbon. *Phys. Rev. B* **2000**, *61*, 14095−14107.
(43) Casiraghi, C.; Pisana, S.; Novoselov, K. S.; Geim, A. K.; Ferrari, A. C. Raman Fingerprint of Charged Impurities in Graphene. *Appl. Phys. Lett.* **2007**, *91*, 233108.
(44) Ferrari, A. C. Raman Spectroscopy of Graphene and Graphite: Disorder, Electron−Phonon Coupling, Doping and Nonadiabatic Effects. *Solid State Commun.* **2007**, *143*, 47−57.
(45) Xie, P.; Wang, Z.; Zhang, Z.; Fan, R.; Cheng, C.; Liu, H.; Liu, Y.; Li, T.; Yan, C.; Wang, N.; Guo, Z. Silica Microsphere Templated Self-Assembly of a Three-Dimensional Carbon Network with Stable Radio-Frequency Negative Permittivity and Low Dielectric Loss. *J. Mater. Chem. C* **2018**, *6*, 5239−5249.
(46) Tuinstra, F.; Koenig, J. L. Raman Spectrum of Graphite. *J. Chem. Phys.* **1970**, *53*, 1126.
(47) Luo, D.; Zhang, G.; Liu, J.; Sun, X. Evaluation Criteria for Reduced Graphene Oxide. *J. Phys. Chem. C* **2011**, *115*, 11327−11335.
(48) Kim, S. S.; Jo, S. B.; Gueon, K. I.; Choi, K. K.; Kim, J. M.; Churn, K. S. Complex Permeability and Permittivity and Microwave Absorption of Ferrite-Rubber Composite at X-Band Frequencies. *IEEE Trans. Magn.* **1991**, *27*, 5462−5464.
(49) Yusoff, A. N.; Abdullah, M. H.; Ahmad, S. H.; Jusoh, S. F.; Mansor, A. A.; Hamid, S. A. A. Electromagnetic and Absorption Properties of Some Microwave Absorbers. *J. Appl. Phys.* **2002**, *92*, 876−882.
(50) Vinoy, K. J.; Jha, R. M. Trends in Radar Absorbing Materials Technology. *Sadhana* **1995**, *20*, 815−850.
(51) Xie, P.; Li, H.; He, B.; Dang, F.; Lin, J.; Fan, R.; Hou, C.; Liu, H.; Zhang, J.; Ma, Y.; Guo, Z. Bio-Gel Derived Nickel/Carbon Nanocomposites with Enhanced Microwave Absorption. *J. Mater. Chem. C* **2018**, *6*, 8812−8822.
(52) Zhang, N.; Huang, Y.; Zong, M.; Ding, X.; Li, S.; Wang, M. Synthesis of ZnS Quantum Dots and $CoFe_2O_4$ Nanoparticles Co-Loaded with Graphene Nanosheets as an Efficient Broad Band EM Wave Absorber. *Chem. Eng. J.* **2017**, *308*, 214−221.
(53) Huang, H.-D.; Liu, C.-Y.; Zhou, D.; Jiang, X.; Zhong, G.-J.; Yan, D.-X.; Li, Z.-M. Cellulose Composite Aerogel for Highly Efficient Electromagnetic Interference Shielding. *J. Mater. Chem. A* **2015**, *3*, 4983−4991.
(54) Han, M.; Yin, X.; Kong, L.; Li, M.; Duan, W.; Zhang, L.; Cheng, L. Graphene-Wrapped ZnO Hollow Spheres with Enhanced Electromagnetic Wave Absorption Properties. *J. Mater. Chem. A* **2014**, *2*, 16403−16409.
(55) Li, X.; Yin, X.; Song, C.; Han, M.; Xu, H.; Duan, W.; Cheng, L.; Zhang, L. Self-Assembly Core-Shell Graphene-Bridged Hollow MXenes Spheres 3D Foam with Ultrahigh Specific EM Absorption Performance. *Adv. Funct. Mater.* **2018**, *28*, 1803938.
(56) He, J.-Z.; Wang, X.-X.; Zhang, Y.-L.; Cao, M.-S. Small Magnetic Nanoparticles Decorating Reduced Graphene Oxides to Tune the

DOI: 10.1021/acsami.8b15416
ACS Appl. Mater. Interfaces 2018, 10, 42865−42874

Electromagnetic Attenuation Capacity. *J. Mater. Chem. C* **2016**, *4*, 7130−7140.
(57) Quan, L.; Qin, F. X.; Estevez, D.; Wang, H.; Peng, H. X. Magnetic Graphene for Microwave Absorbing Application: Towards the Lightest Graphene-Based Absorber. *Carbon* **2017**, *125*, 630−639.
(58) Chen, C.; Xi, J.; Zhou, E.; Peng, L.; Chen, Z.; Gao, C. Porous Graphene Microflowers for High-Performance Microwave Absorption. *Nano-Micro Lett.* **2018**, *10*, 26.
(59) Zhao, H.; Han, X.; Li, Z.; Liu, D.; Wang, Y.; Wang, Y.; Zhou, W.; Du, Y. Reduced Graphene Oxide Decorated with Carbon Nanopolyhedrons as an Efficient and Lightweight Microwave Absorber. *J. Colloid Interface Sci.* **2018**, *528*, 174−183.
(60) Yan, F.; Guo, D.; Zhang, S.; Li, C.; Zhu, C.; Zhang, X.; Chen, Y. An Ultra-Small $NiFe_2O_4$ Hollow Particle/Graphene Hybrid: Fabrication and Electromagnetic Wave Absorption Property. *Nanoscale* **2018**, *10*, 2697−2703.
(61) Yang, R.; Wang, B.; Xiang, J.; Mu, C.; Zhang, C.; Wen, F.; Wang, C.; Su, C.; Liu, Z. Fabrication of $NiCo_2$-Anchored Graphene Nanosheets by Liquid-Phase Exfoliation for Excellent Microwave Absorbers. *ACS Appl. Mater. Interfaces* **2017**, *9*, 12673−12679.
(62) Yang, Y.; Xia, L.; Zhang, T.; Shi, B.; Huang, L.; Zhong, B.; Zhang, X.; Wang, H.; Zhang, J.; Wen, G. Fe_3O_4@LAS/RGO Composites with a Multiple Transmission-Absorption Mechanism and Enhanced Electromagnetic Wave Absorption Performance. *Chem. Eng. J.* **2018**, *352*, 510−518.
(63) Zhang, D.; Jia, Y.; Cheng, J.; Chen, S.; Chai, J.; Yang, X.; Wu, Z.; Wang, H.; Zhang, W.; Zhao, Z.; Han, C.; Cao, M.; Zheng, G.-P. High-Performance Microwave Absorption Materials Based on MoS_2-Graphene Isomorphic Hetero-Structures. *J. Alloys Compd.* **2018**, *758*, 62−71.

DOI: 10.1021/acsami.8b15416
ACS Appl. Mater. Interfaces 2018, 10, 42865−42874